Physics of the Earth and Planetary Interiors 280 (2018) 20–31

Contents lists available at ScienceDirect

Physics of the Earth and Planetary Interiors

journal homepage: www.elsevier.com/locate/pepi

Co-seismic deformation following the 2007 Bengkulu earthquake constrained by GRACE and GPS observations

Zengji Zheng[a,c,d], Shuanggen Jin[b,a,*], Lihong Fan[e]

[a] Shanghai Astronomical Observatory, Chinese Academy of Sciences, Shanghai 200030, China
[b] School of Remote Sensing and Geomatics Engineering, Nanjing University of Information Science and Technology, Nanjing 210044, China
[c] University of Chinese Academy of Sciences, Beijing 100049, China
[d] Shaanxi Earthquake Agency, Xi'an 710068, China
[e] National Time Service Center, Chinese Academy of Science, Xi'an 710600, China

ARTICLE INFO

Keywords:
Seismic deformation
Fault slip
GRACE
GPS

ABSTRACT

Gravity changes caused by giant earthquakes can be detected by Gravity Recovery and Climate Experiment (GRACE), which provide new constraints on earthquake ruptures. However, detailed rupture, seismic moment and density/displacement-induced gravity changes are not clear for less than Mw = 8.5 earthquakes. In this paper, the fault parameters of the 2007 Mw = 8.4 Bengkulu earthquake are retrieved from GRACE and GPS data, and the fault slip distribution is inverted using GPS data. Furthermore, the theoretical coseismic displacements and coseismic gravity changes from different slip models are compared with GPS and GRACE data. The results show that the significant positive and negative gravity anomalies with a peak magnitude of −2.0 to 1.3 μgal are extracted from GRACE data. The GRACE-inverted and joint-inverted seismic moment of the Bengkulu earthquake are 3.27×10^{21} Nm and 3.30×10^{21} Nm with the rake angle of 108° and 114°, respectively. The GPS-inverted Mw = 8.4 earthquake is mainly dominated by the thrusting with slight right-lateral strike-slip, which is consistent with the focal mechanism. GRACE-observed coseismic gravity changes agree well with the results from the fault models based on the spherically dislocation theories in spatial pattern, but are larger than model-estimated results in magnitude. The coseismic gravity changes caused by the density change are basically same as those caused by the vertical displacement in the magnitude of order, which are −0.8 to 0.2 μgal and −0.2 to 1.4 μgal for the Caltech model, −0.9 to 0.2 μgal and −0.5 to 1.3 μgal for the USGS model, and −0.9 to 0.2 μgal and −0.3 to 1.3 μgal for the GPS-inverted layered model. In addition, both the near-field and the far-field displacements calculated from the Caltech model and GPS-inverted layered model are in good agreement with the GPS observations, whereas the USGS model has good agreement in the far-field and poor agreement in the near-field with the GPS observations, especially in the Pagai Selatan area.

1. Introduction

With the launch of the Gravity Recovery and Climate Experiment (GRACE) mission since 2002, it has been very successful to monitor the Earth's time-variable gravity field and to measure mass redistribution, such as terrestrial water storage and Earth Rotation excitation (Jin and Feng, 2013; Jin et al., 2011; Jin and Zhang, 2012), ice sheet mass balance and sea level change (Jin et al., 2016; Jin and Zou, 2015). Besides, GRACE observations have improved our understanding of the largest earthquakes (Han, 2006). Since the signal generated by most earthquakes is small when compared with the background noise, only several giant earthquakes were successfully observed, e.g., the 2004 Mw = 9.3 Sumatra–Andaman earthquake (Chen et al., 2007; Han, 2006), 2010 Mw = 8.8 Maule (Chile) earthquake (Han et al., 2010; Wang et al., 2012), 2011 Mw = 9.0 Tohoku-Oki (Japan) earthquake (Dai et al., 2014; Fuchs et al., 2016; Li et al., 2016), 2012 Mw = 8.7 Indian Ocean earthquake (Han et al., 2015) and 2013 Mw = 8.3 Okhotsk earthquake (Tanaka et al., 2015; Zhang et al., 2016). Among them, only the 2013 Mw = 8.3 Okhotsk earthquake was less than Mw = 8.5. Although the 2006 Mw = 8.3 thrust and 2007 Mw = 8.1 normal fault earthquakes in the central Kuril Islands resulted in significant postseismic gravity changes, coseismic gravity changes were not discernible from GRACE measurements (Han et al., 2016).

For large undersea earthquakes, GRACE data have been demonstrated to have the feasibility to complement other data for detecting and constraining fault parameters, since GRACE data have a better

* Corresponding author.
E-mail addresses: sgjin@shao.ac.cn, sg.jin@yahoo.com (S. Jin).

https://doi.org/10.1016/j.pepi.2018.04.009
Received 1 March 2018; Received in revised form 9 April 2018; Accepted 21 April 2018
Available online 23 April 2018
0031-9201/

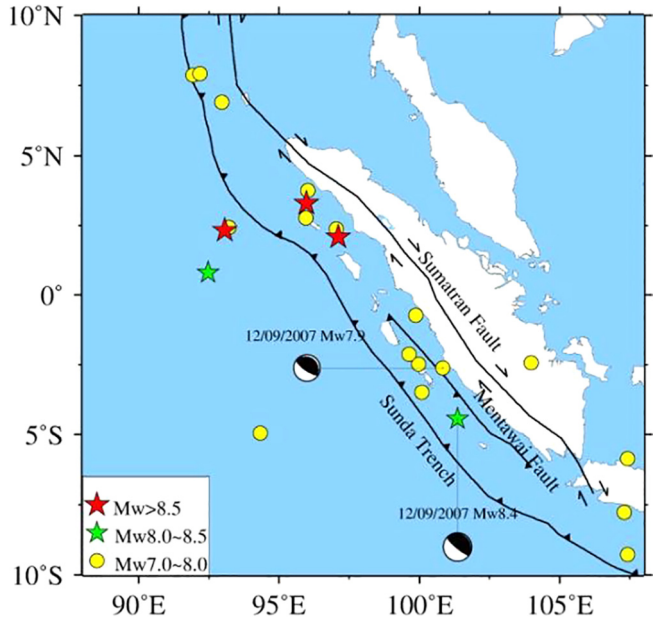

Fig. 1. Earthquakes in the broad Sumatran plate boundary region from 2004 to 2016. The earthquakes data and centroid-moment tensor (CMT) solutions were from the US Geological Survey (USGS) Earthquake Catalog (https://earthquake.usgs.gov/earthquakes/).

spatial coverage at global scale when compared to Global Positioning System (GPS) data and seismic data (Cambiotti et al., 2011; Cambiotti and Sabadini, 2013; Dai et al., 2016; Dai et al., 2014; Fuchs et al., 2016; Han et al., 2013; Han et al., 2011; Wang et al., 2012). The moment tensor of a point source can be solved based on normal mode formulation (Cambiotti et al., 2011; Cambiotti and Sabadini, 2013; Han et al., 2011, 2013; Dai et al., 2016). Wang et al. (2012) and Dai et al. (2014) retrieved fault parameters based on a rectangular finite fault model. However, the extension of the rupture were poorly constrained by GRACE data because of low spatial resolution (Cambiotti and Sabadini, 2012). In the estimation of slip distribution and crustal structure, GPS, gravity and seismic data are jointly used (Gusman et al., 2010; Konca et al., 2008; Jin and Park 2006; Tenzer et al., 2015).

The Sunda-Andaman megathrust is one of the most seismically active structures in the world. The oblique subduction is manifested principally by two large-scale subparallel tectonic structures—the Sumatran strike-slip fault and the Sunda megathrust. From 2004 to 2016, the Sumatran plate boundary (Fig. 1) experienced three Mw = 8.5, two Mw = 8, and seventeen Mw = 7 earthquakes. On 12 September 2007, the Bengkulu Mw = 8.4 earthquake occurred in the west of southern Sumatra. About 12 h later, a deeper Mw = 7.9 earthquake occurred next to the northeastern edge of the main rupture of Mw = 8.4 earthquake. The Mw = 8.4 Bengkulu earthquake in Sumatra marked the first in a modern series of large earthquakes along the Mentawai section of the Sunda megathrust.

Unlike other places dominated by one or two earthquakes, the Sumatra–Andaman subduction zone is punctuated by many earthquakes that were often embedded within the postseismic decay of previous earthquakes. The postseismic decays of several earthquakes frequently overlap each other. Therefore, it is challenge to identify the true coseismic deformation of the Bengkulu earthquake. Furthermore, the limited spatial resolution of GRACE (~350 km spatial resolution with degree 60 truncation of spherical harmonic coefficients) and a little magnitude of the Bengkulu earthquake with respect to the 2004 Sumatra–Andaman Mw = 9.3 earthquake make it difficult to retrieve seismic signals from GRACE. Previous studies have observed coseismic displacement and postseismic slip using limited GPS, but it has lack of observations in ocean areas (Feng et al., 2015; Konca et al., 2008; Lubis et al., 2013; Tsang et al., 2016). Although synthetic gravity changes of the 2007 Bengkulu earthquake was computed based on centroid moment tensor (CMT) solutions inversed from GRACE monthly data (Han et al., 2013), no one retrieved obvious coseismic gravity changes directly from the GRACE L2 data.

In this paper, coseismic gravity changes of the 2007 Bengkulu earthquake are extracted from GRACE time-variable gravity field for the first time. In order to better understand the fault mechanism, the fault parameters of the 2007 Bengkulu earthquake are retrieved from GRACE and GPS observations and the slip distribution was inverted using GPS observations. Furthermore, we compared theoretical coseismic displacements and coseismic gravity changes from different slip models based on the spherically dislocation theories (Sun et al., 2010) with GPS and GRACE observations. In addition, gravity changes induced by density changes and vertical displacements were separated and investigated from the coseismic gravity changes of the 2007 Bengkulu earthquake calculated from fault slip models.

2. Observation data and models

2.1. GRACE data

GRACE Level-2 RL05 monthly data in term of spherical harmonic coefficients up to degree 60 released by the University of Texas Center for Space Research (CSR) were used here. Compared with GRACE RL04 data, the noise of GRACE RL05 data has been reduced significantly. The degree 2 order 0 (C20) coefficients in the GRACE data were replaced by estimates obtained from satellite laser ranging (Cheng and Tapley, 2004). Monthly geocenter estimates calculated by Swenson et al. (2008) were used to account for the degree 1 coefficients of the gravity field, which GRACE does not observe.

The gravity changes from the GRACE gravitational models can be expressed as

$$\Delta g(r,\theta,\lambda) = \frac{GM}{R^2}\sum_{n=0}^{N}(n-1)\left(\frac{R}{r}\right)^2\sum_{m=0}^{n}[\Delta\overline{C}_{nm}cos m\lambda + \Delta\overline{S}_{nm}sin m\lambda]\cdot \overline{P}_{nm}(cos\theta) \quad (1)$$

where GM is the geocentric gravitational constant, R is the mean equatorial Earth radius, $r = a(1-f\cos^2\theta)$ is radius vector on the ellipsoid, θ and λ are the colatitude and longitude, respectively, $\Delta\overline{C}_{nm}$, $\Delta\overline{S}_{nm}$ are the residual stoke coefficients with respect to the mean gravity field, and $\overline{P}_{nm}$ are the fully normalized associated Legendre Polynomials of degree n and order m. The spherical harmonic coefficients are converted into grid gravity changes with a resolution of 0.25°.

In order to suppress the stronger noises in the higher-degree SH (spherical harmonic) coefficients and north–south stripes due to the correlated errors among the even- or odd degree coefficient pairs of the same order, P3M6 decorrelation and Gaussian smoothing with 300 km radius were applied (Chen et al., 2007; Wahr et al., 1998).

2.2. GPS observations

The coseismic deformation observed by GPS was used from Feng et al. (2015). The nonlinear curve fitting was used to systematically analyze the SuGAr (Sumatran GPS Array) daily position time series for the period from August 2002 to the end of 2013, and the coseismic displacements and postseismic decays, along with long-term rates and seasonal signals were simultaneously estimated in the fitting. SuGAr stations data were processed using the GIPSY-OASIS version 6.2. In the processing, tidal effects from ocean, pole, and solid Earth tides were modeled and corrected, and any postprocessing filtering to the daily solutions were avoid. Here, we used 18 cGPS (continuous GPS) stations which recorded coseismic offsets of the 2007 Bengkulu earthquake.

Table 1
Parameters of different finite models.

Agency	Earthquake	Length/km	Width/km	Strike/°	Dip/°	Data adopted
USGS	Mw8.4	352	320	320	15	47 P waveforms 35 SH waveforms 87 long period surface waves
	Mw7.9	224	162.15	317.3	25	19 P waveforms 16 SH waveforms 40 long period surface waves
Caltech	Mw8.4	400	368	324	15	16P waveforms 19 SH waveforms 37 GPS measurements 1 L-band ALOS PALSAR interferogram
	Mw7.9	240	190	323	15	19 P waveforms 17 SH waveforms 27 GPS measurements

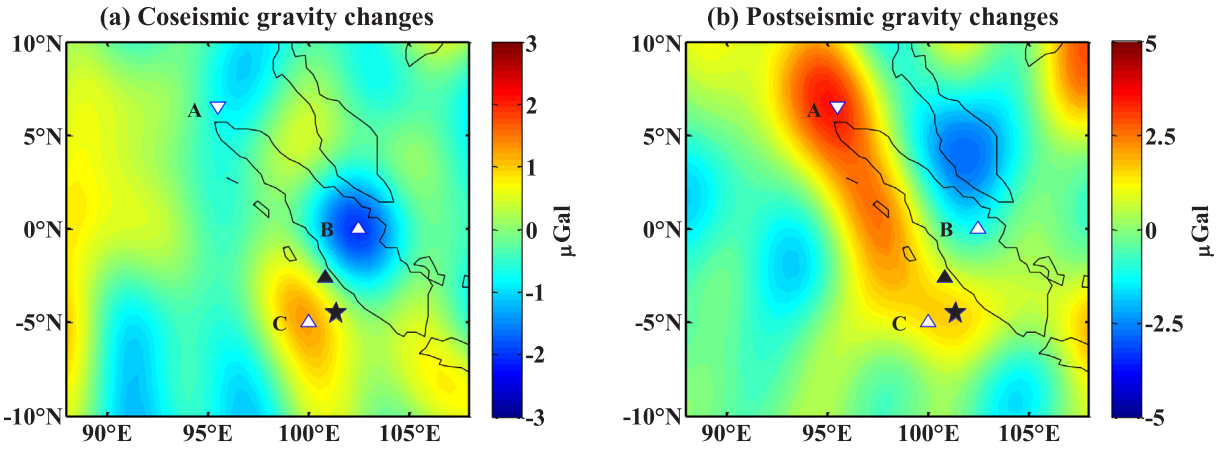

Fig. 2. The coseismic and postseismic gravity changes associated with the 2007 Bengkulu earthquake. (a) Coseismic gravity changes by time-series fitting of 3.5 years data. (b) Postseismic gravity changes by time-series fitting. The black pentagram and triangles indicate the Mw8.4 and Mw7.9 epicenter, respectively. The white lower triangle is the point with maximum positive postseismic gravity changes. Two white upper triangles are characteristic points in Fig. 3.

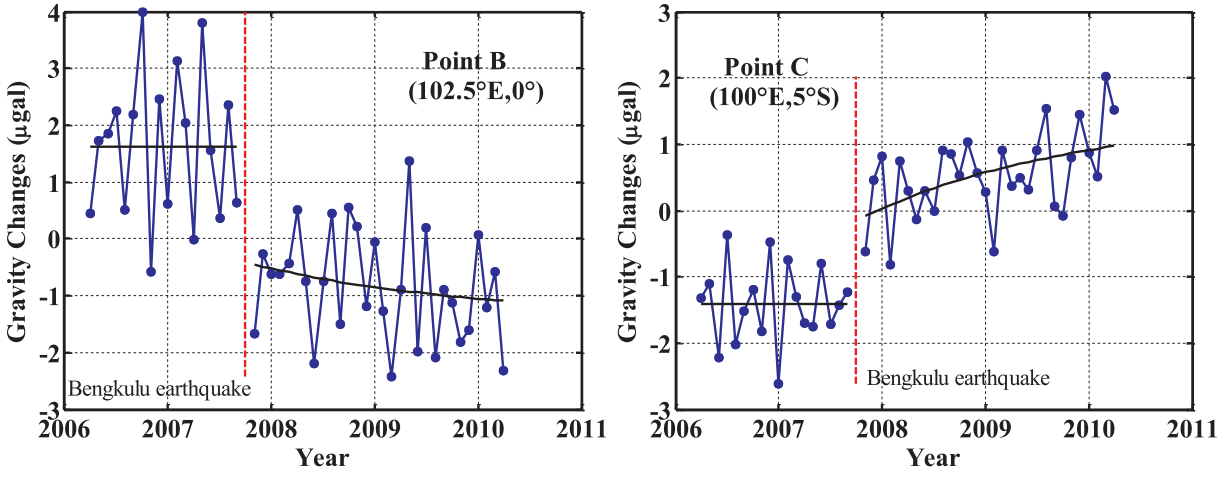

Fig. 3. Time-series of gravity changes at point B and point C in Fig. 2a. The annual and semiannual terms were removed. The red vertical dashed line denotes the occurrence day of the earthquake (12 September 2007).

Table 2
The set of initial parameters for inversion.

Fault Parameters	Minimum	Maximum	Unit
Length	0	600	km
Width	0	400	km
Slip	0	10	M
Rake angle	70	150	Deg

2.3. Finite fault models

After the Bengkulu earthquake occurred, a number of fault slip models were obtained. In this paper, fault models released by Caltech (California Institute of Technology) (http://www.tectonics.caltech.edu/slip_history/) and the USGS (United States Geological Survey) (https://earthquake.usgs.gov/earthquakes/eventpage/official20070912111026830_34#finite-fault) were used, respectively.

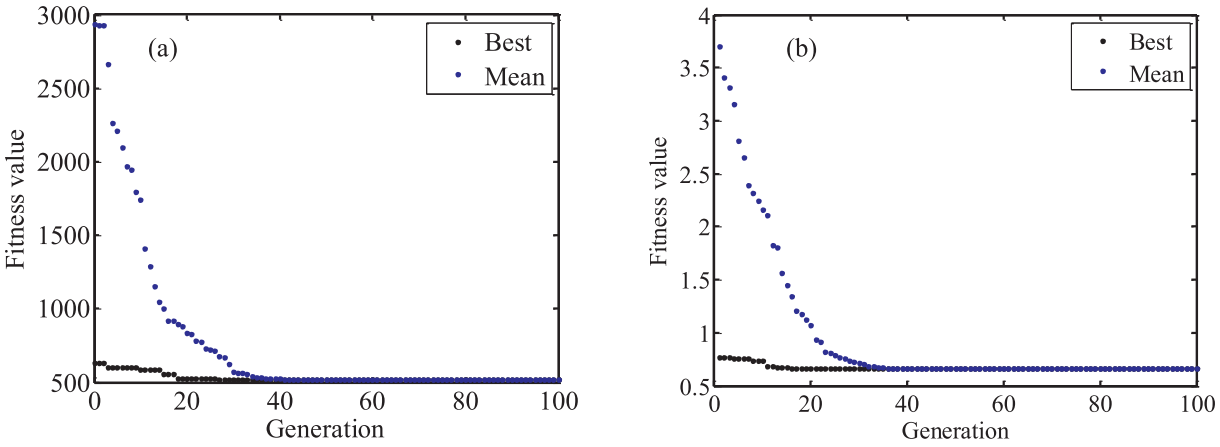

Fig. 4. Convergence curves of the cost function. (a) and (b) are convergence curves of GRACE-inverted and joint-inverted results, respectively. The blue and black dots represent the mean and best value of the cost function in each generation of particles.

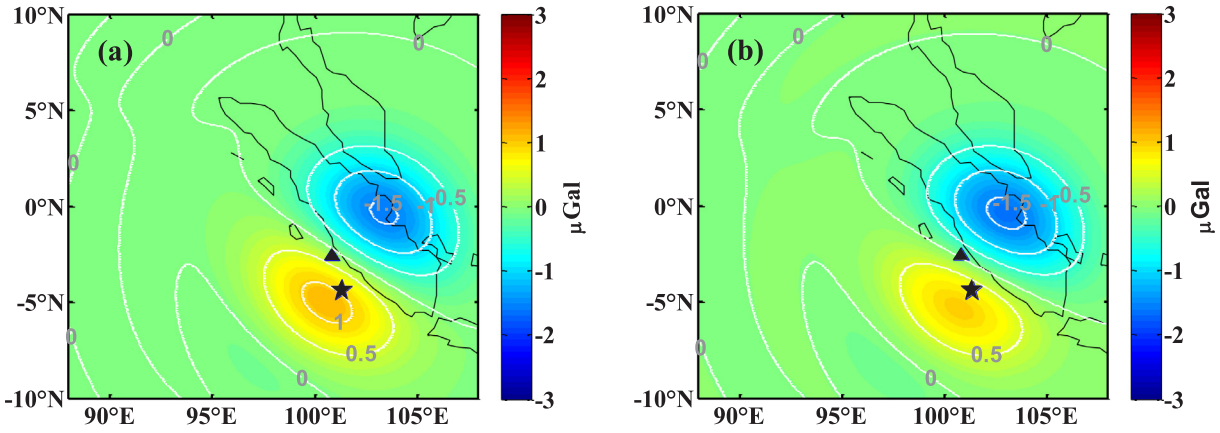

Fig. 5. The coseismic gravity changes calculated from inverted fault parameters. (a) and (b) are coseismic gravity changes calculated from GRACE-inverted and joint-inverted fault parameters, respectively.

Table 3
Crust velocity-density structure.

depth/km	V_p/(km·s^{-1})	V_s/(km·s^{-1})	density/(g·cm^3)
0.00	2.20	0.78	2000
1.30	2.20	0.78	2000
5.62	6.00	3.50	2720
12.10	6.60	3.80	2860
22.89	7.10	3.90	3050
⩾ 22.89	7.99	4.40	3300

For the convenience of expression, the fault models are named by the source organizations, Caltech model and USGS model, respectively. Due to the assumed geometrical models, the data used are different when two fault models were inverted, and the resulting slip distribution are correspondingly different. The USGS model mainly used seismic data, while the Caltech model used not only seismic data but also geodetic data, such as GPS and InSAR (Interferometric Synthetic Aperture Radar) data. The specific parameters of each model are shown Table 1.

3. Theory and methods

3.1. Particle Swarm Optimization (PSO) algorithm

The Particle Swarm Optimization (PSO) algorithm (Kennedy and Eberhart, 1995) was applied to estimate fault parameters in this paper. The PSO algorithm is a global optimization method inspired by the social behavior of individuals in nature (swarms) that has been successfully used in many different disciplines (Fatolazadeh et al., 2017; Martínez et al., 2010; Pallero et al., 2017). In the inversion for geophysical problems with a low number of parameters and fast forward problems, PSO is a very powerful stochastic algorithm. Moreover, compared to other optimal algorithm such as Simulated Annealing (SA) and Genetic Algorithms (GA), PSO is fast in terms of convergence rate (Martínez et al., 2010).

In PSO, a number of simple individuals or particles that represent a potential solution to an optimization problem are placed in the search space of the problem, and each evaluates the objective function at its current location. Each particle then determines its movement through the search space by combining its own current and best (best-fitness) locations with those of one or more members of the swarm. The next iteration takes place after all particles have been moved, eventually the swarm moves close to an optimum of the fitness function (Poli et al., 2007).

PSO algorithm consists of the following steps (Eberhart and Kennedy, 2002; Shi and Eberhart, 1998):

1) Initialization: Initialize an array of particles with random position x^0 and velocities v^0 in d dimensional problem space;
2) Evaluation: For each particle, evaluate the desired optimization fitness function;
3) Velocity updating: In every iteration, the velocities of all particles are updated according to

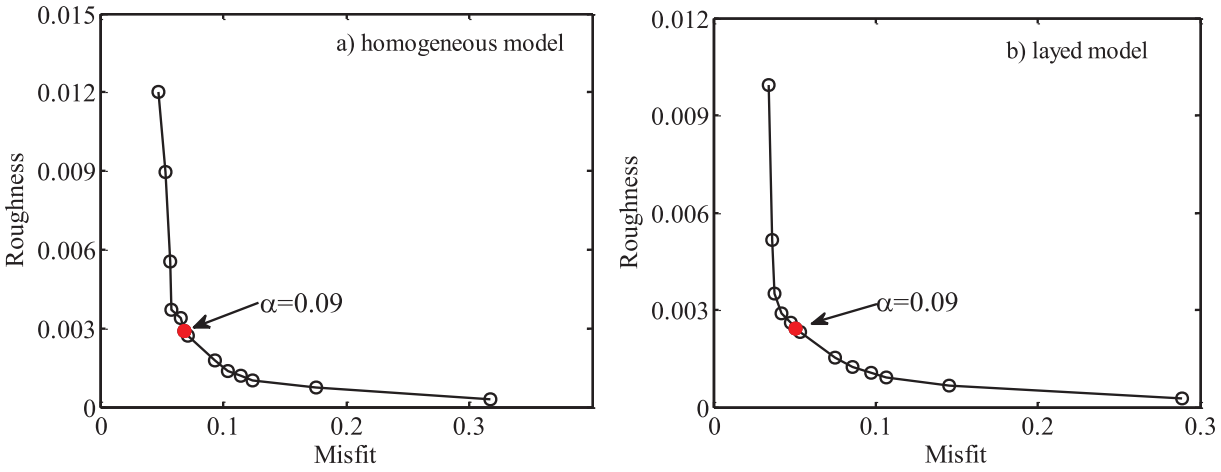

Fig. 6. Trade-off curve between model roughness and data misfit.

Table 4
Comparison of different source slip models.

model name	mean slip/m	slip and location				Mw
		maximum slip/m	latitude/°	longitude/°	depth/km	
Homogeneous model	0.62	7.55	−3.25	100.35	27.34	8.22
Layed model	0.56	6.75	−3.25	100.35	27.34	8.31
Caltech Mw8.4 model	0.56	9.60	−3.23	100.25	25.28	8.40

$$V_{id}(k+1) = \omega V_{id}(k) + c_1 r_1 (pbest_{id}(k) - x_{id}(k)) + c_2 r_2 (gbest_d(k) - x_{id}(k)) \quad (2)$$

where $x_{id}(k)$ and $V_{id}(k)$ are the position and velocity of particle i in d dimensional space respectively, ω is a real constant called inertia weight, c_1 and c_2 are accelerating factor, r_1 and r_2 are random variables uniformly distributed in [0,1], $pbest_{id}(k)$ is the best position of particle i in d dimensional space until generation k, and $gbest_d(k)$ is the best position of the whole swarm in d dimension until generation k;

4) Position updating: Between successive iterations, the position of all particles is updated according to

$$x_{id}(k+1) = x_{id}(k) + V_{id}(k+1) \quad (3)$$

where $x_{id}(k+1)$ and $V_{id}(k+1)$ are the new position and new velocity, respectively.

5) Memory updating: Update particle best position $pbest_{id}(k)$ and global best position $gbest_d(k)$ using equation

$$\begin{cases} pbest_{id}(k+1) = x_{id}(k+1) & if\ f(x_{id}(k+1)) < f(pbest_{id}(k)) \\ gbest_d(k+1) = x_{id}(k+1) & if\ f(x_{id}(k+1)) < f(gbest_d(k)) \end{cases} \quad (4)$$

where $f(x)$ is the objective function to be minimized.

6) Repeat from Step 3 to Step 5 until the criterion is satisfied (usually a sufficiently good fitness or a maximum number of iterations).

3.2. The steepest descent method

The problem of fault slip distribution inversion can be described as:

$$Y = Gb + \varepsilon \quad (5)$$

where Y is the observation vector, G is the Green function, which is related to the selected media model such as homogeneous elastic half-space model or multi-layered elastic half-space model, b is the fault slip vector, and ε is the errors between observations and slip model.

In order to obtain optimal fault dislocation model, the fault plane is usually discretized into some regular rectangular sub-faults, and then the slip amount of each sub-fault is calculated to obtain the dislocation distribution of the whole fault. However, discretizing the fault plane into a number of sub-faults will result in a significant increase in the number of unknown parameters. When the parameters of the fault to be determined are larger than the number of observations, the derived slip distribution may exhibit an unrealistic oscillatory character. To solve this problem, some artificial constraints such as restricting the maximum slip amplitude and the minimum and maximum rake angles are usually used. To make the slip solution stable and reasonable, here we adopt a constrained least squares method proposed by Wang et al. (2004) to invert for the slip models. Besides, the steepest descent method was applied to search for the optimal solution, and the cost function was defined as (Wang et al., 2009):

$$F(b) = \|Y - Gb^2\| + \alpha^2 \|Hs^2\| = w_1 \left\| \frac{d_1 - d_1^0 - Gb^2}{\delta_1} \right\| + w_2 \left\| \frac{d_2 - d_2^0 - Gb^2}{\delta_1} \right\| + \cdots + \alpha^2 \left(\left\| \frac{\partial^2}{\partial x^2} Hs^2 \right\| + \left\| \frac{\partial^2}{\partial y^2} Hs^2 \right\| \right) \quad (6)$$

where α is the smoothing factor, which controls the trade-off between model roughness and data misfit, H is the finite difference approximation of the Laplacian operator, s is the slip amplitude of each sub-fault on the fault plane, d_i is different datasets, d_i^0 is unknown data offsets, δ_i is absolute error, and w_i is relative weights between different datasets.

4. Results and analysis

4.1. Coseismic gravity changes from GRACE

In order to suppress the contaminations of GRACE data from seasonal variations and estimate coseismic deformation, we adopted the least squares fitting method to extract coseismic gravity changes. To mitigate the postseismic impact of the 2004 Sumatra Mw = 9.3 earthquake and the preseismic impact of the Sumatra Mw = 7.8 earthquake on 6 April 2010, the GRACE data were used from March 2006 to March 2010, which is 1.5 years before the earthquake and 2.5 years after the earthquake. During the time-series fitting, we applied an annual, a semi-annual term as the periodic changes, 161 day S2 tidal wave term before and after the earthquake, respectively, a linear trend term before the earthquake and a postseismic relaxation term after the earthquake, which could be expressed as following (de Linage et al., 2009):

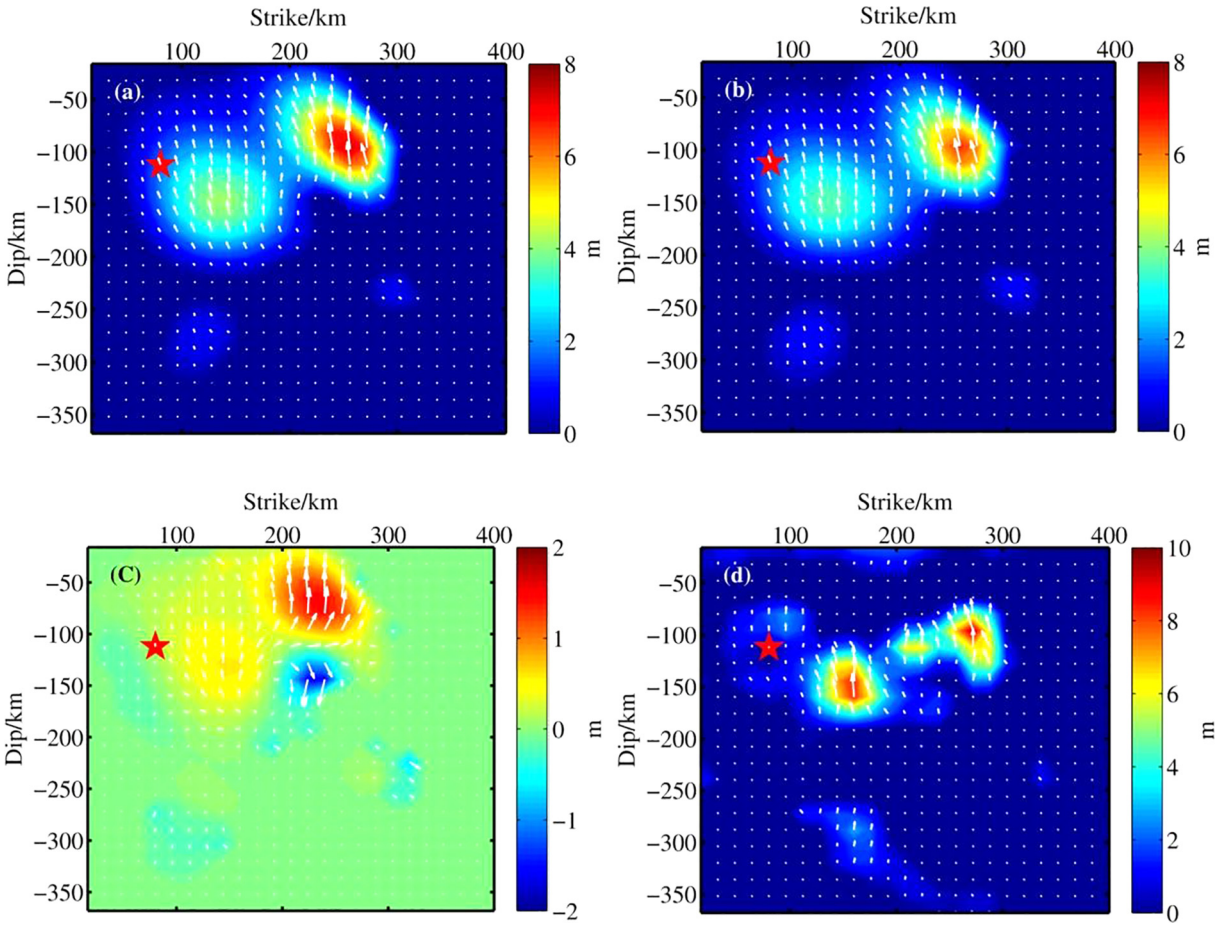

Fig. 7. The slip distribution on fault plane of Mw8.4 earthquake. (a) and (b) are the slip distribution using homogeneous half-space model and layered half-space model, respectively; (c) is the difference between (a) and (b); (d) is the slip distribution of Caltech Mw8.4 model. The red star indicates the hypocenter location of the Mw8.4 earthquake. The colors show the slip amplitude and white arrows indicate the direction of motion of the hanging wall relative to the footwall.

$$y(t) = \sum_{i=1}^{3} a_i \cos(\omega_i t + \phi_i) + \begin{cases} c_1 + bt & ,t < t_{eq} \\ c_2 + d(1-e^{-(t-t_{eq}/\tau)}) & ,t > t_{eq} \end{cases} \quad (7)$$

where a_1, ϕ, a_2, ϕ_2, a_3, ϕ_3 are the amplitudes and phases of the annual, semi-annual and 161 day S2 tidal waves to model the seasonal and annual variations of hydrology and long-peirod oceanic circulations, b is a linear trend before earthquake, c_2-c_1 is the coseismic jump, τ and d are the relaxation time and total postseismic gravity changes reached at the end of the relaxation. Here, the 3.5-year GRACE gravity time series were fitted at each grid point (with grid cell size of 0.25° × 0.25°).

The postseismic relaxation time is crucial for the correct extraction of the coseismic and postseismic gravity changes. As the postseismic gravity changes was significant, the minimum residual standard deviation method was usually adopted to calculate the relaxation time (Li et al., 2016; Tanaka and Heki, 2014). At first, we calculated the relaxation time at point A (95.5°E, 6.5°N) (Fig. 2b) with maximum positive postseismic gravity changes but we found that the relaxation time did not converge, which may be due to tectonic movement. Therefore, we calculated the relaxation factor at the point C (100°E, 5°S) with the positive peak of coseismic gravity change and the relaxation constant is equal to 2.1. Fig. 2(a) and (b) show the coseismic and postseismic gravitational changes calculated by the least squares fitting.

As shown in Fig. 2(a), although a wide range of negative anomalous regions (probably affected by GRACE noise) appeared in the northwest of the epicenter, the coseismic gravity changes was successfully extracted. The characteristics of postseismic gravity changes are "negative-positive-negative", of which the positive variation ranged from the epicenter to the northwest of North Sumatra along the coastline, and negative anomalies were on both sides.

In order to observe the time-varying characteristics of gravity changes, time series of gravitational changes were calculated at the positive and negative peak points (B (102.5°E, 0°) and C (100°E, 5°S) as shown in Fig. 2a). During the calculation, the annual and semiannual period terms signals and the effects of S2 tidal wave were removed, as shown in Fig. 3. There are significant jumps before and after the Bengkulu earthquake in both uplift and subduction zones. The magnitude of change in the subduction zone (point B, ~1.9 μgal of gravity change) is more significant than that in the uplift zone (point A, ~1.3 μgal of gravity change).

4.2. Fault parameters from GRACE and GPS

The quantification of large undersea earthquakes is critical for improving our understanding of fault mechanisms. Here, we use the GRACE-observed coseismic gravity changes described in Section 4.1 and GPS-observed coseismic displacements from Feng et al. (2015) to solve fault parameters. Because of Okubo's and Okada's mathematical simplicity in computing gravity changes (Okada, 1985; Okubo, 1992), a homogenous elastic half-space model with uniform slip on the fault plane is assumed for the study. Since GRACE-observed gravity can provide excellent constraints on the fault strike angle, dip angle, fault width, fault length, rake angle, dislocation magnitude, and less sensitive to fault depth (Dai et al., 2014), we fixed the depth during our

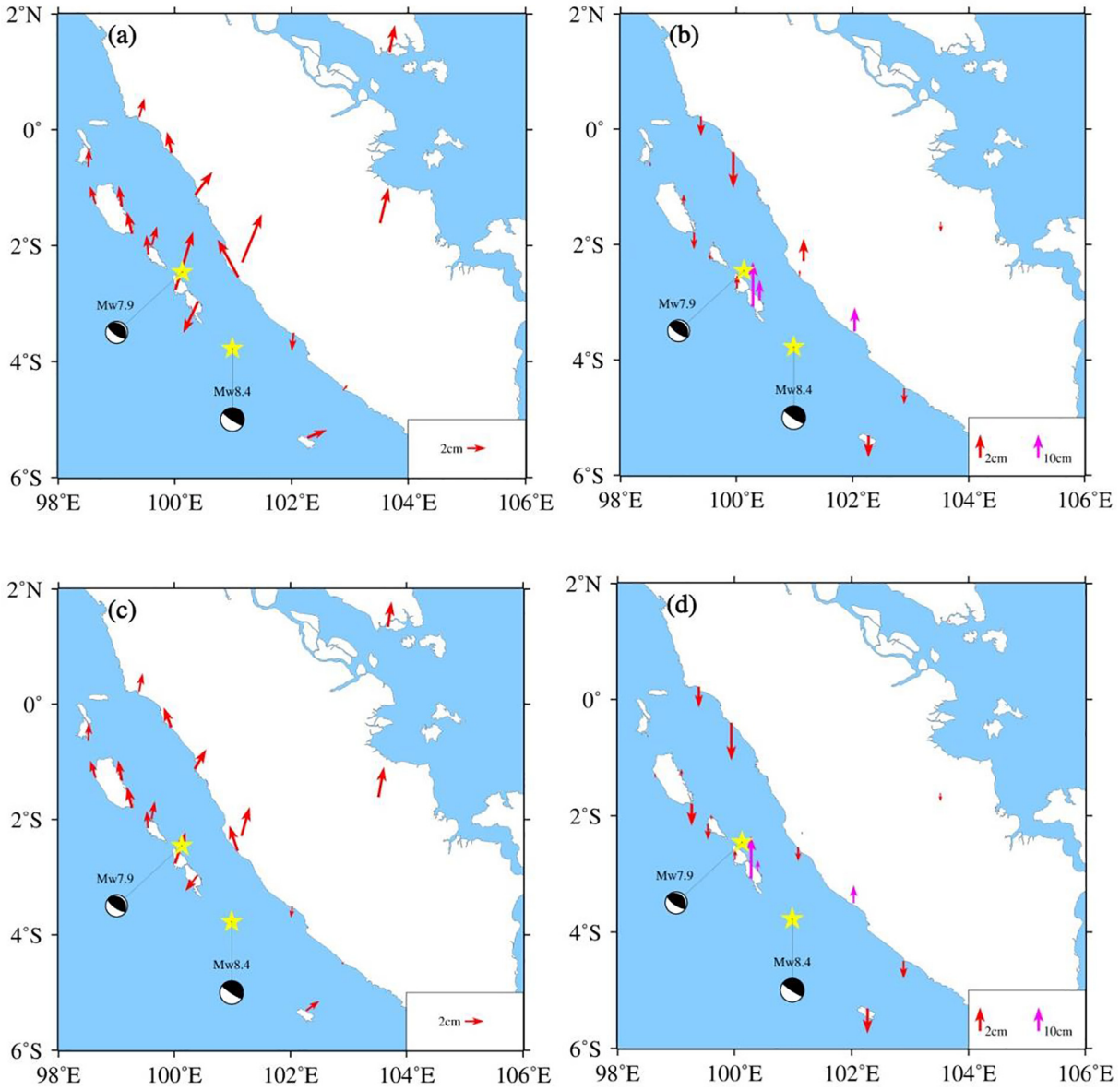

Fig. 8. Horizontal and vertical residuals of coseismic offsets. (a) and (c) are horizontal residuals in the homogeneous model and layered model, respectively; (b) and (d) are vertical residuals in the homogeneous model and layered model, respectively.

inversion. In addition, the strike and dip angle are well constrained by the plate boundary direction and centroid-moment tensor solutions, so we fixed the strike and dip angle.

The PSO algorithm is applied to simultaneously estimate fault-plane length, width, average slip magnitude and the rake angle, with the strike angle fixed at 324°, dip angle fixed at 15°, and the depth of the top edge of the fault fixed at 5 km. The cost function (energy function) is defined as the sum of squares of the differences between model predictions and GRACE-observed gravity changes and GPS-observed displacements changes. In order to speed up the convergence rate, we applied some artificial constraints on the inversion parameters (See Table 2). Firstly, the fault parameters are inversed using only GRACE data, and the fault length, width, the average slip and rake angle are estimated as 401 km, 358 km, 0.76 m and 108°, respectively. Assuming a mean rigidity of 30 GPa, the new GRACE-derived total seismic moment is 3.27×10^{21} Nm, resulting in a moment-magnitude Mw = 8.31.

Furthermore, the fault parameters are jointly inversed using GRACE and GPS data. In order to scale the amplitudes of each data set, a ratio of the L2 norms of the observation vectors was used as the weight factor for joint inversion of GRACE and GPS data (Xu et al., 2009). The weight scaling factor can be solved by

$$\frac{1-\lambda}{\lambda} = \frac{\|\varepsilon_{ob}\|}{\|u_{0b}\|} \quad \text{or} \quad \frac{1-\lambda}{\lambda} = \frac{\sigma_1^2}{\sigma_2^2} \tag{8}$$

where λ and $1-\lambda$ are the weight scaling factor of the GRACE and GPS data, respectively; $\|\varepsilon_{ob}\|$ and $\|u_{ob}\|$ denote the L2 norm of the GRACE-observed gravity changes and GPS-observed displacement changes, respectively; σ_1^2 and σ_2^2 are the squares of the standard errors of GRACE-observed gravity changes and GPS-observed displacement changes, respectively. Here, we estimate the GRACE error by using the mean square root (RMS) of residuals extracted by the least squares fitting which described in Section 4.1 (Wahr et al., 2006), and the calculated λ is equal to 0.82. The inversion result can be evaluated by the relative difference of model prediction compared to GRACE and GPS observation, which could be expressed as following (Dai et al., 2014)

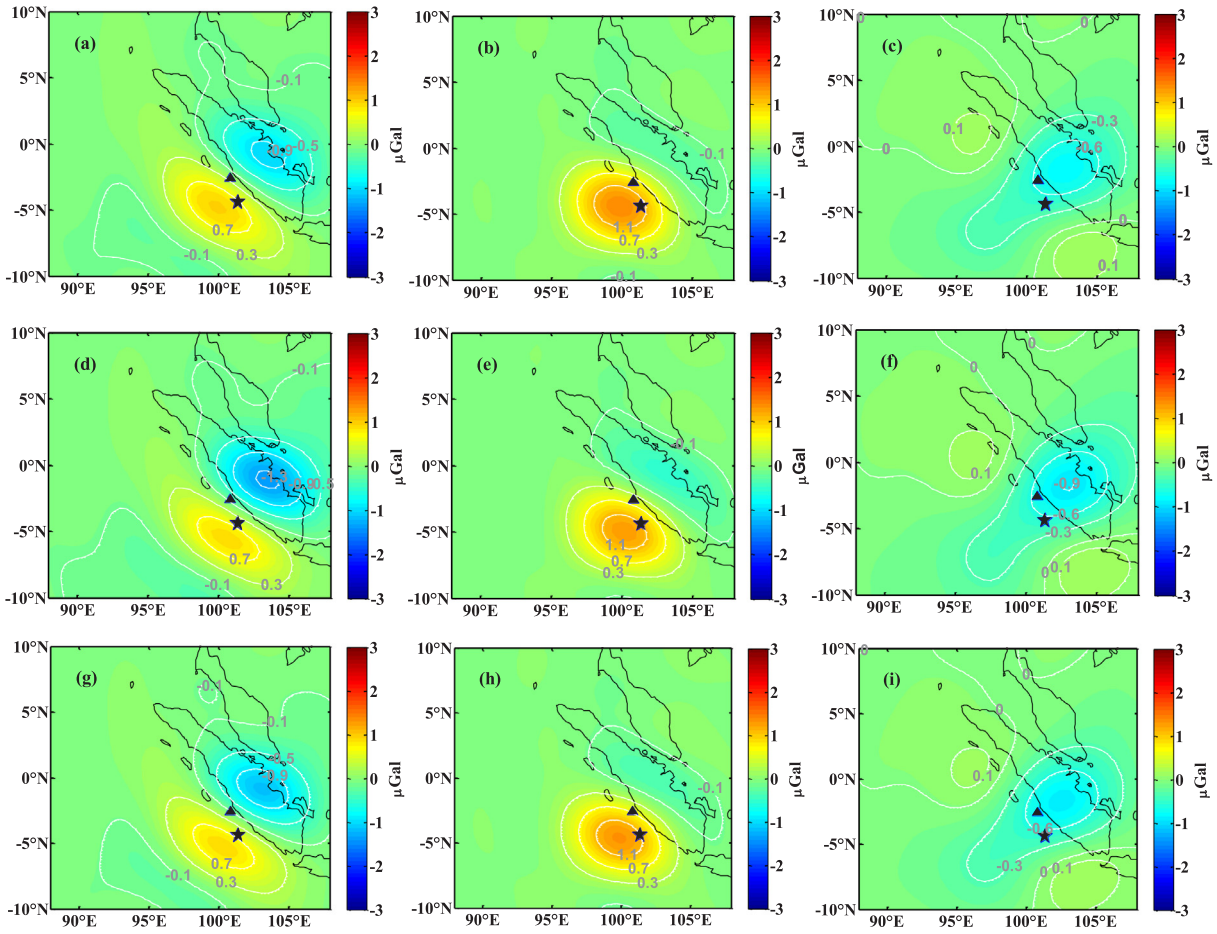

Fig. 9. The coseismic gravity changes calculated from Caltech model USGS model and GPS-inverted layered model. (a), (d) and (g) are total gravity changes with sea water correction from Caltech model, USGS model and GPS-inverted layered model, respectively. (b), (e) and (h) are gravity changes caused by vertical displacement from Caltech model, USGS model and GPS-inverted layered model, respectively. (c), (f) and (i) are gravity changes caused by density redistribution from Caltech model, USGS model and GPS-inverted layered model, respectively.

$$Rd = \frac{\sqrt{\sum_{i=1}^{n1} (ob_{GRACE}(x,y) - m_1(x,y))^2 / n1}}{\sqrt{\sum_{i=1}^{n1} ob_{GRACE}(x,y)^2 / n1}} + \frac{\sqrt{\sum_{i=1}^{n2} (ob_{Gps}(x,y) - m_2(x,y))^2 / n2}}{\sqrt{\sum_{i=1}^{n2} ob_{GPS}(x,y)^2 / n\,2}} \quad (9)$$

where Rd denotes the relative difference, (x,y) are the coordinates of the observation points, n1 and n2 are the number of GRACE and GPS observation points, respectively, ob_{GRACE} and ob_{GPS} denote GRACE-observed gravity changes and GPS-observed displacements, respectively, m_1 and m_2 denote model-predicted gravity changes and displacement. The joint-inverted fault length, width, the average slip and rake angle are estimated as 427 km, 330 km, 0.78 m and 114°, respectively, and the corresponding total seismic moment is 3.30×10^{21} Nm, resulting in a moment-magnitude Mw = 8.31.

Since *Rd* calculated from GRACE-inverted results and joint-inverted results are 1.5 and 1.0, respectively, the accuracy of joint inversion results is increased by 50% relative to GRACE inversion results. Fig. 4 shows the convergence curves of the cost function. Fig. 5 shows the coseismic gravity changes calculated from inverted fault parameters. As shown in Fig. 4, the PSO algorithm converges very quickly, and convergence is basically completed around 40 generations.

4.3. Fault slip distribution of the Mw8.4 earthquake from GPS

To obtain the dislocation distribution of the 2007 Mw = 8.4 mainshock, we used the coseismic GPS data to invert the coseismic slip distribution of the Bengkulu earthquake based on SDM software (Wang et al., 2009; Wang et al., 2013). The SDM software inverts the coseismic slip distribution based on the constrained least-squares principle and the steepest descent method, which has been widely used. In the inversion process, the geometry of the rupture is consistent with Caltech Mw = 8.4 earthquake. The fault strike angle and the dip angle were fixed at 324°and 15°, respectively. The fault plane was divided into 25 × 23 sub-faults and each sub-fault was 16 km × 16 km in area. 1D crustal model was interpolated from CRUST1.0 (https://igppweb.ucsd.

Table 5
Coseismic gravity changes of fault models caused by different factors.

Model name	Total gravity changes/μgal	Gravity changes caused by displacement/μgal	Gravity changes caused by density μgal
Caltech model	−1.0 to 1.0	−0.2 to 1.4	−0.8 to 0.2
USGS model	−1.4 to 0.9	−0.5 to 1.3	−0.9 to 0.2
Layered model	−1.1 to 0.9	−0.3 to 1.3	−0.9 to 0.2

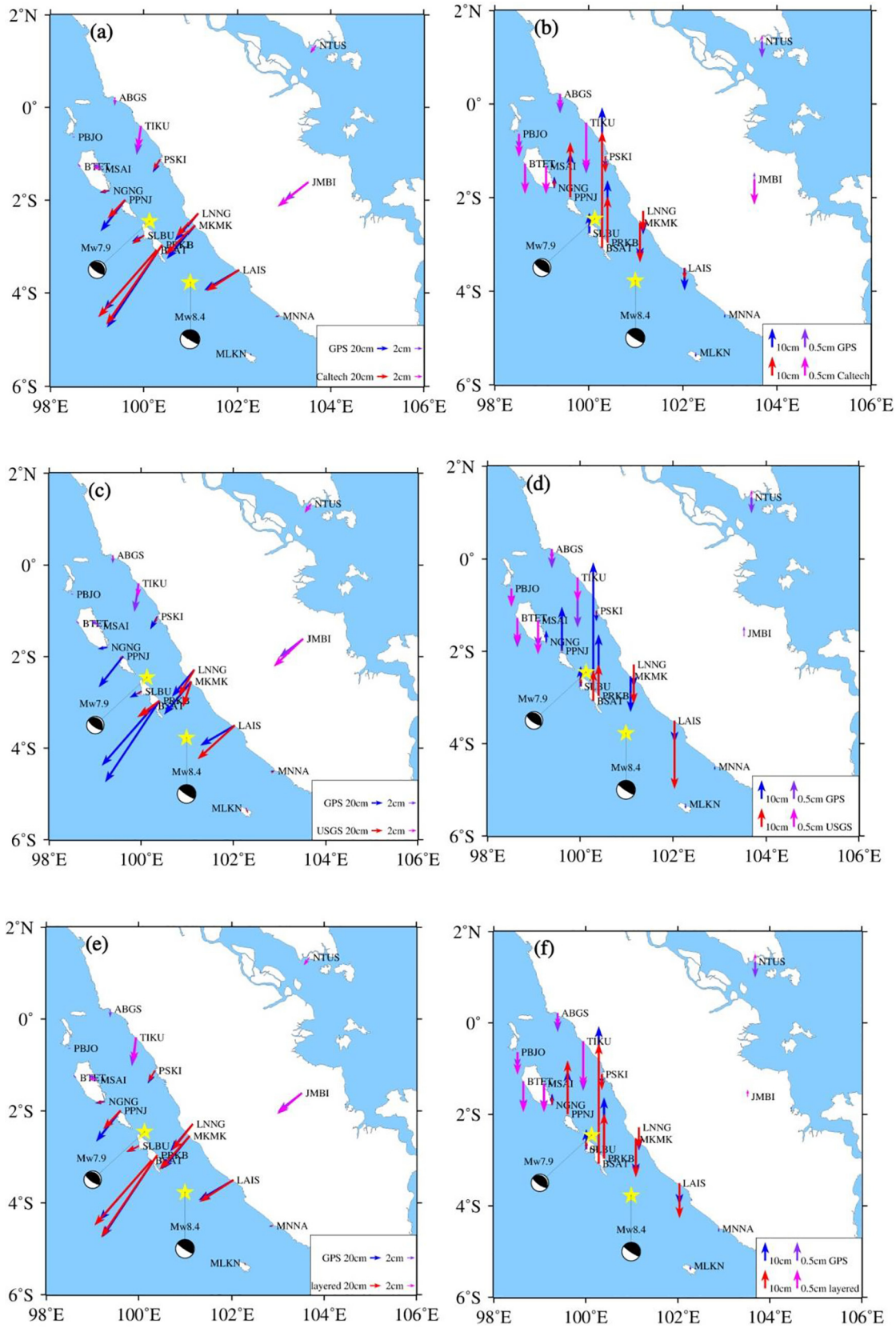

Fig. 10. The coseismic displacements calculated from Caltech model, USGS model and GPS-inverted layered model. (a), (c) and (e) are coseismic horizontal displacements from Caltech model, USGS model, and GPS-inverted layered model respectively. (b), (d) and (f) are coseismic vertical displacements from Caltech model, USGS model and GPS-inverted layered model, respectively.

edu/~gabi/crust1.html), which was showed in Table 3. In order to determine optimal fault slip distribution, we used the trade-off curve between the model roughness and data misfit to determine smoothing factor α. And the final smoothing factor α is 0.09, as shown in Fig. 6.

Table 4 and Fig. 7 illustrate the sip distribution inversed from the homogenous half-space model and the layered half-space model. As shown in Table 4, the inversed results from the homogeneous model and the layered model are basically the same. The average and maximum slip amplitudes inversed from the homogeneous model are marginally larger than the layered model, the maximum difference between them is up to 1.5 m (Fig. 7c), but the location of maximum slip is the same. The maximum slippage (7.55 m and 6.75 m) and moment magnitude (Mw = 8.22 and Mw = 8.31) retrieved by using only the GPS data are less than the maximum slippage (9.60 m) and moment magnitude (Mw = 8.40) of Caltech Mw = 8.4 model, which was derived from the joint inversion of GPS, InSAR and seismic waveforms data, and the maximum slips are located deeper than those from the joint inversion. In addition, from the slip distribution of the earthquake rupture (Fig. 7), it can be clearly seen that the earthquake is a thrust event with slightly right-lateral strike-slip, which shows general agreement with the focal mechanisms of this earthquake. After the earthquake, it ruptured northwest along the fault strike direction. The maximum rupture point is not near the hypocenter, but about 180 km northwest of the hypocenter.

Fig. 8 shows the residual distribution between GPS observation and the models. The RMS errors in three orientations (East, North and Up) are 1.2, 2.9 and 5.5 cm for the homogeneous model, and 0.7, 2.1 and 4.7 cm for layered model, respectively. The RMS error of the layered model is less than the homogeneous model, which may be due to that the layered model is closer to the real earth structure.

4.4. Coseismic gravity changes from fault slip models

In order to judge the GRACE results, the simulated coseismic gravity changes surrounding Bengkulu earthquake on the space-fixed points were computed by the spherical dislocation theory (Sun et al., 2010). Since the coseismic gravity changes observed by GRACE include both the Mw = 8.4 earthquake and the Mw = 7.9 earthquake, the above two fault models must be included in the comparison of theoretical simulation results.

To compare the results observed by GRACE, firstly, the simulation results were expanded into coefficients of spherical harmonics with degrees and orders up to 60 and secondly, spherical harmonic coefficients are filtered using the 300 km Gaussian smoothing filter and P3M6 decorrelation as GRACE data processed. It should be noted that the gravitational effect induced by the seawater disturbance needs to be further considered. The presence of ocean dramatically reduces the density discontinuity at the solid Earth's surface (from about 2600 kg/m3 to 1600 kg/m3), and consequently reduces the gravity signal due to topographic changes. Here we treated the seawater disturbance as an incompressible burger layer with thickness as same as seafloor displacements, calculated its gravity disturbance and then corrected them from the original results, as suggested by Zhou et al. (2011). The correction model is expressed as:

$$\delta g^{total} = \delta g^{solid} - 2\pi G\rho_w h Q(\theta,\lambda) \tag{10}$$

$$Q(\theta,\lambda) = \begin{cases} 1 & (\theta,\lambda) \in Ocean \\ 0 & (\theta,\lambda) \in Land \end{cases} \tag{11}$$

where δg^{total} and g^{solid} are the corrected and original model-predicted gravity changes, respectively, G is the gravitational constant, h is the vertical displacement of seafloor calculated by the dislocation theory, and $Q(\theta,\lambda)$ is the ocean function. The magnitude of seawater loading displacements is less than seawater disturbance that can be neglected. Since the RMS error of the GPS-inverted layered model is less than the homogeneous model, here we select the layered model to compute theoretical coseismic gravity changes. Fig. 9(a), (d) and (g) illustrate simulated coseismic gravity changes calculated from Caltech model, USGS model and GPS-inverted layered model, respectively. It is obvious that model-simulated coseismic gravity changes (Fig. 9a, d and g) are smaller than the GRACE-observed results (Fig. 2a) but with the same spatial pattern. The amplitude of coseismic gravity calculated by Caltech model, USGS model and GPS-inverted layered model are −1.0 to 1.0μgal, −1.4 to 0.9μgal and −1.1 to 0.9μgal, respectively. The actual amplitude of the coseismic gravity changes observed by GRACE (Fig. 2a) are −2.0 to 1.3μgal. In terms of magnitude of the coseismic gravity changes, the USGS model results are closer to GRACE than other two models, but in terms of amplitude, all of them are smaller than GRACE with maximum difference up to 1 μgal.

The major factors contributing to the coseismic gravity signal are density changes within the Earth's upper layers and the displacement of rock material. When modeling the gravity changes observed by GRACE, the role of density variations is found to be as large as that of the vertical displacement, especially for an earthquake with a shallow focus (~20 km) (Tanaka et al., 2015). Here, we calculated the gravity changes caused by vertical displacement (Fig. 9b, e and h) and the gravity changes caused by density changes (Fig. 9c, f and i), from the Caltech model, the USGS model, and GPS-inverted layered model, respectively. The gravity changes due to vertical displacement are determined by:

$$\delta g^{vertical} = 2\pi G\rho_{crust} h(\theta,\lambda) 10^8 \tag{12}$$

where $\delta g^{vertical}$ is gravity changes due to vertical displacement, ρ_{crust} is the average crustal density ($2700 kg/m^3$), $h(\theta,\lambda)$ are the vertical displacements. The effect of seawater disturbance should also be considered. The results of the statistics are shown in Table 5. Table 5 shows that the magnitude of the coseismic gravity changes caused by the vertical displacements is basically the same as those caused by the density change, which is consistent with the result of Tanaka's study (Tanaka et al., 2015). In the west of the epicenter, the gravity changes are dominated by vertical displacement, while in the east of the epicenter, gravity changes are dominated by the density changes.

4.5. Coseismic displacement from fault slip models

The coseismic displacements of 18 GPS stations (Fig. 10) were also calculated using the spherical dislocation theory and compared with the actual GPS observations provided by Feng et al. (2015). The differences between theoretical simulation results and GPS observations were statistically analyzed using mean square root (RMS) from the following equation:

$$\sigma = \sqrt{\frac{1}{N}\sum_{i=1}^{N}(u_{cal} - u_{GPS})^2} \tag{13}$$

where N is the number of stations, u_{cal} and u_{GPS} are the horizontal or vertical displacements of the corresponding points from fault models and GPS, respectively. Table 6 shows the statistical results and Fig. 10 shows the coseismic displacements calculated from Caltech model and USGS model.

As shown in Table 6 the calculated values from Caltech model are

Table 6
Mean square roots of differences between fault models and GPS.

Model	RMS(σ/m)		
	east-west	south-north	vertical
Caltech	0.04	0.07	0.05
USGS	0.25	0.38	0.17
Layered	0.01	0.02	0.05

Table 7
Comparison of Source Parameters.

Model name	Data sources	Rake/°	$M_0/10^{21}$ Nm
Konca et al., 2008	GPS, SAR, Teleseismic data	99	5.00
GCMT	Seismic waves	114	6.71
USGS CMT	Seismic waves	103	5.30
Han et al., 2013	CSR RL04	–	5.00
Dai et al., 2016	OSU	108	3.09
	CSR RL05	72	3.16
	GFZ RL05a	80	4.16
This study	CSR RL05	108	3.27
	CSR RL05, GPS	114	3.30

more reasonable agreement with the GPS observations, and the accuracy of the Caltech model is one order of magnitude better than the USGS model. As shown in Fig. 10, directions of the coseismic horizontal displacements in both the GPS and fault models were uniformly trenchward, while the directions of coseismic vertical displacements showed downward, apart from large uplift of Pagai Selatan, Pagai Utara, and Sipura island.

The displacements from the Caltech model are in good agreement with the GPS observations in both the near-field and the far-field. However, the USGS model is well consistent with the GPS observations only in the far-field, and poorly consistent in the near-field, especially in the Pagai Selatan area. The reason is that the Caltech model used a large amount of GPS data during the inversion, while the USGS model only used the seismic data. Furthermore, the afterslip of the Bengkulu earthquake was large (Feng et al., 2016). The seismic wave only reflects the fault slip process at the occurrence of the earthquake and cannot constrain the total amount of slip of the earthquake. Since the layered model based on only the GPS data during the inversion, the simulated-result of layered model is in best agreement with the GPS observations.

5. Discussions

The low spatial resolution (200 km–350 km) and limited temporal resolution (monthly intervals) make it difficult to retrieve the weak seismic signals from GRACE. The seismic signals observed by GRACE only represent the long wavelength part of the seismic deformation. To better retrieve seismic signals, a longer record of GRACE data (before and after the earthquake) is needed. But this will inevitably introduce some contamination between coseismic and postseismic effects. Furthermore, any filtering approach will likely depress or distort true signals while suppressing noises.

Although fault slip models are usually used to verify the seismic signals retrieved by GRACE, large discrepancies up to 1 μgal in Bengkulu earthquake still exist. The difference can be ascribed to the following reasons: 1) A single relaxation factor was adopted to extract the coseismic signal from the least squares fitting method. Studies have shown that the relaxation time varies throughout the region, but it is not certain whether this change is due to the relaxation of the true postseismic mass variation or GRACE errors (Li et al., 2016). Moreover, postseismic gravity changes include afterslip, viscoelastic relaxation and pore fluid adjustment, and here we only simulated viscoelastic relaxation effect. 2) Fault models are not accurate. Table 5 shows that parameters (fault length, width, strike and dip) of different finite models are different, and it is difficult to judge which model is more accurate. The maximum difference between the Caltech and USGS model is up to 0.5 μgal, accounting for 50% of the difference between the fault model and the GRACE observations. 3) Compared with the 2004 Sumatra Mw = 9.3 earthquake and the 2011 Japan Mw = 9.1 earthquake, the magnitude and coseismic changes signals of the Bengkulu earthquake are relatively small, and the corresponding noise caused by ocean and atmosphere disturbance are relatively large, so the errors are relatively large.

Table 7 shows the fault parameters retrieved by different agencies and researchers. Since the fault length, width and slip amplitude jointly determine the seismic moment, only the rake angle and the seismic moment of the fault are compared here. We can see that the divergence for fault parameters from different products is large, e.g. the difference is up to 42° for rake angle and 3.62×10^{21} Nm for seismic moment. The GRACE-inverted rake angle in this study is consistent with that in Dai et al. (2016) inverted from OSU products, and joint-inverted rake angle is consistent with the GCMT inverted from seismic waves. However, even with the same CSR RL05 data, the rake angle retrieved by this study is 36° larger than that by Dai et al. (2016). This may be related to the inversion algorithm and data processing strategy. Furthermore, the relatively small rupture plane and large surrounding noise (large-scale negative anomalies in the northwest of the epicenter) will affect the inversion results. In terms of seismic moment, GRACE-inverted and joint-inverted M_0 are overall smaller than that from GCMT and USGS CMT solution, whereas the result of Han et al. (2013) is consistent with that in Konca et al. (2008). The GRACE-inverted M_0 in this paper is 1.73×10^{21} Nm smaller than that in Han et al. (2013) with the least discrepancy to that in Dai et al. (2016) using the same CSR RL05 data. Since Han et al. (2013) adopted the Slepian basis function method which maximum preserves the seismic signal and improves the signal-to-noise ratio by avoiding any filtering, the seismic moment retrieved by Han is the largest in all GRACE products and closest to the CMT solution.

Although GRACE can provide excellent constraints on the fault parameters, owing to low spatial resolution (almost equal to the fault length of the 2007 Bengkulu earthquake), GRACE is not appropriate for inversion of fault slip distribution. As a result, during the inversion for fault sip distribution, we used only GPS data. As we described in Section 2.3, most studies used seismic wave data and geodetic data (include GPS and InSAR data). The slip fault models inversed from multiple data are often better than those merely using GPS data. With respect to earthquakes occurred in ocean, GPS stations are always distributed on the one side and far from the epicenter, the inverted model can only provide a general survey of the slip distribution due to the incompleteness of observations and the non-uniqueness in the inversion (Diao et al., 2012). If more near-field observational data are introduced into the slip distribution inversion, the spatial resolution of the inversed slip fault would be improved. Finally, the effects of lateral heterogeneity and topography also affect inversion result.

6. Conclusions

In this paper, the coseismic gravity changes signal of the 2007 Bengkulu earthquake are the first time extracted successfully from the GRACE Level-2 data. Through the comparison with the model-simulated gravity changes using spherical dislocation theory, the GRACE results are almost consistent. Furthermore, for an earthquake with a shallow focus (~20 km), the coseismic gravity changes caused by vertical displacements have same magnitude as those from the density rearrangement. This paper shows that GRACE satellites have the ability to detect earthquakes with moment magnitudes $M_W < 8.5$.

In addition, GRACE directly observes gravity changes above the fault area that can provide independent constraint on the earthquake source parameters, whereas GPS can well estimate fault slip distribution. Thus, GRACE and GPS data can complement each other for a robust inversion of the seismic source of large earthquakes. The GRACE-inverted and joint-inverted seismic moment of the Bengkulu earthquake are 3.27×10^{21} Nm and 3.30×10^{21} Nm with the rake angle of 108° and 114°, respectively. The GPS-inverted Mw = 8.4 earthquake is mainly dominated by the thrusting with slight right-lateral strike-slip. In the future, we will jointly inverse the fault slip distribution from multi-satellite observation data.

Acknowledgments

We are grateful to the CSR for providing GRACE data. We also appreciate the generosity of Lujia Feng (Nanyang Technological University, Singapore) with sharing their GPS data and Dr. Rongjiang Wang (GFZ German Research Centre for Geosciences, Germany) for giving enthusiasm guidance in the use of SDM software. This work was supported by the National Natural Science Foundation of China (NSFC) Project (Grant No. 11373059).

Appendix A. Supplementary data

Supplementary data associated with this article can be found, in the online version, at http://dx.doi.org/10.1016/j.pepi.2018.04.009.

References

Cambiotti, G., Bordoni, A., Sabadini, R., Colli, L., 2011. GRACE gravity data help constraining seismic models of the 2004 Sumatran earthquake. J. Geophys. Res. 116. http://dx.doi.org/10.1029/2010jb007848.

Cambiotti, G., Sabadini, R., 2012. A source model for the great 2011 Tohoku earthquake (Mw = 9.1) from inversion of GRACE gravity data. Earth Planet. Sci. Lett. 335–336, 72–79. http://dx.doi.org/10.1016/j.epsl.2012.05.002.

Cambiotti, G., Sabadini, R., 2013. Gravitational seismology retrieving Centroid-Moment-Tensor solution of the 2011 Tohoku earthquake. J. Geophys. Res. Solid Earth 118, 183–194. http://dx.doi.org/10.1029/2012jb009555.

Chen, J.L., Wilson, C.R., Tapley, B.D., Grand, S., 2007. GRACE detects coseismic and postseismic deformation from the Sumatra-Andaman earthquake. Geophys. Res. Lett. 34. http://dx.doi.org/10.1029/2007gl030356.

Cheng, M., Tapley, B.D., 2004. Variations in the Earth's oblateness during the past 28 years. J. Geophys. Res. 109.

Dai, C., Shum, C.K., Guo, J., Shang, K., Tapley, B., Wang, R., 2016. Improved source parameter constraints for five undersea earthquakes from north component of GRACE gravity and gravity gradient change measurements. Earth Planet. Sci. Lett. 443, 118–128. http://dx.doi.org/10.1016/j.epsl.2016.03.025.

Dai, C., Shum, C.K., Wang, R., Wang, L., Guo, J., Shang, K., Tapley, B., 2014. Improved constraints on seismic source parameters of the 2011 Tohoku earthquake from GRACE gravity and gravity gradient changes. Geophys. Res. Lett. 41, 1929–1936. http://dx.doi.org/10.1002/2013gl059178.

de Linage, C., Rivera, L., Hinderer, J., Boy, J.-P., Rogister, Y., Lambotte, S., Biancale, R., 2009. Separation of coseismic and postseismic gravity changes for the 2004 Sumatra-Andaman earthquake from 4.6 yr of GRACE observations and modelling of the coseismic change by normal-modes summation. Geophys. J. Int. 176, 695–714. http://dx.doi.org/10.1111/j.1365-246X.2008.04025.x.

Diao, F.Q., Xiong, X., Zheng, Y., 2012. Static slip model of the M_w 9.0 Tohoku (Japan) earthquake: results from joint inversion of terrestrial GPS data and seafloor GPS/acoustic data. Chin. Sci. Bull. 57, 1990–1997.

Eberhart, R., Kennedy, J., 2002. A new optimizer using particle swarm theory. In: International Symposium on MICRO Machine and Human Science, pp. 39–43.

Fatolazadeh, F., Naeeni, M.R., Voosoghi, B., Rahimi, A., 2017. Estimation of fault parameters using GRACE observations and analytical model: case study: the 2010 Chile earthquake. J. Geodyn. 108, 26–39. http://dx.doi.org/10.1016/j.jog.2017.05.004.

Feng, L., Barbot, S., Hill, E.M., Hermawan, I., Banerjee, P., Natawidjaja, D.H., 2016. Footprints of past earthquakes revealed in the afterslip of the 2010 Mw 7.8 Mentawai tsunami earthquake. Geophys. Res. Lett. 43, 9518–9526.

Feng, L., Hill, E.M., Banerjee, P., Hermawan, I., Tsang, L.L.H., Natawidjaja, D.H., Suwargadi, B.W., Sieh, K.E., 2015. A unified GPS-based earthquake catalog for the Sumatran plate boundary between 2002 and 2013. J. Geophys. Res. 120, 3566–3598.

Fuchs, M.J., Hooper, A., Broerse, T., Bouman, J., 2016. Distributed fault slip model for the 2011 Tohoku-Oki earthquake from GNSS and GRACE/GOCE satellite gravimetry. J. Geophys. Res. Solid Earth 121, 1114–1130. http://dx.doi.org/10.1002/2015jb012165.

Gusman, A.R., Tanioka, Y., Kobayashi, T., Latief, H., Pandoe, W., 2010. Slip distribution of the 2007 Bengkulu earthquake inferred from tsunami waveforms and InSAR data. J. Geophys. Res. Solid Earth 115.

Han, S.-C., Riva, R., Sauber, J., Okal, E., 2013. Source parameter inversion for recent great earthquakes from a decade-long observation of global gravity fields. J. Geophys. Res. Solid Earth 118, 1240–1267. http://dx.doi.org/10.1002/jgrb.50116.

Han, S.-C., Sauber, J., Luthcke, S., 2010. Regional gravity decrease after the 2010 Maule (Chile) earthquake indicates large-scale mass redistribution. Geophys. Res. Lett. 37. http://dx.doi.org/10.1029/2010gl045449.

Han, S.-C., Sauber, J., Pollitz, F., 2015. Coseismic compression/dilatation and viscoelastic uplift/subsidence following the 2012 Indian Ocean earthquakes quantified from satellite gravity observations. Geophys. Res. Lett. 42, 3764–3772. http://dx.doi.org/10.1002/2015gl063819.

Han, S.-C., Sauber, J., Pollitz, F., 2016. Postseismic gravity change after the 2006–2007 great earthquake doublet and constraints on the asthenosphere structure in the central Kuril Islands. Geophys. Res. Lett. 43, 3169–3177. http://dx.doi.org/10.1002/2016gl068167.

Han, S.-C., Sauber, J., Riva, R., 2011. Contribution of satellite gravimetry to understanding seismic source processes of the 2011 Tohoku-Oki earthquake. Geophys. Res. Lett. 38. http://dx.doi.org/10.1029/2011gl049975.

Han, S.C., 2006. Crustal dilatation observed by GRACE after the 2004 Sumatra-Andaman earthquake. Science 313, 658–662. http://dx.doi.org/10.1126/science.1128661.

Jin, S.G., Park, P.H., 2006. Strain accumulation in South Korea inferred from GPS measurements. Earth Planets Space 58 (5), 529–534. http://dx.doi.org/10.1186/BF03351950.

Jin, S.G., Zhang, X.G., 2012. Variations and geophysical excitation of Earth's dynamic oblateness estimated from GPS, OBP, and GRACE. Chin. Sci. Bull. 57 (36), 3484–3492. http://dx.doi.org/10.1360/972011-1934.

Jin, S.G., Zhang, L., Tapley, B.D., 2011. The understanding of length-of-day variations from satellite gravity and laser ranging measurements. Geophys. J. Int. 184 (2), 651–660. http://dx.doi.org/10.1111/j.1365-246X.2010.04869.x.

Jin, S.G., Feng, G., 2013. Large-scale variations of global groundwater from satellite gravimetry and hydrological models, 2002–2012. Global Planet. Change 106, 20–30. http://dx.doi.org/10.1016/j.gloplacha.2013.02.008.

Jin, S.G., Tian, X., Feng, G., 2016. Recent glacier changes in the Tien Shan observed by satellite gravity measurements. Global Planet. Change 143, 81–87. http://dx.doi.org/10.1016/j.gloplacha.2016.06.006.

Jin, S.G., Zou, F., 2015. Re-estimation of glacier mass loss in Greenland from GRACE with correction of land–ocean leakage effects. Glob. Planet. Change 135, 170–178. http://dx.doi.org/10.1016/j.gloplacha.2015.11.002.

Kennedy, J., Eberhart, R.C., 1995. In: Particle Swarm Optimization, International Symposium on Neural Networks, pp. 1942–1948.

Konca, A.O., Avouac, J., Sladen, A., Meltzner, A.J., Sieh, K.E., Fang, P., Li, Z., Galetzka, J., Genrich, J., Chlieh, M., 2008. Partial rupture of a locked patch of the Sumatra megathrust during the 2007 earthquake sequence. Nature 456, 631–635.

Li, J., Chen, J.L., Wilson, C.R., 2016. Topographic effects on coseismic gravity change for the 2011 Tohoku-Oki earthquake and comparison with GRACE. J. Geophys. Res. Solid Earth 121, 5509–5537. http://dx.doi.org/10.1002/2015jb012407.

Lubis, A.M., Hashima, A., Sato, T., 2013. Analysis of afterslip distribution following the 2007 September 12 southern Sumatra earthquake using poroelastic and viscoelastic media. Geophys. J. Int. 192, 18–37.

Martínez, J.L.F., Gonzalo, E.G., Álvarez, J.P.F., Kuzma, H.A., Pérez, C.O.M., 2010. PSO: a powerful algorithm to solve geophysical inverse problems: application to a 1D-DC resistivity case. J. Appl. Geophys. 71, 13–25.

Okada, Y., 1985. Surface deformation due to shear and tensile faults in a half-space. Bull. Seismol. Soc. Am. 75, 1018–1040.

Okubo, S., 1992. Gravity and potential changes due to shear and tensile faults in a half-space. J. Geophys. Res. Solid Earth 97, 7137–7144.

Pallero, J.L.G., Fernández-Martínez, J.L., Bonvalot, S., Fudym, O., 2017. 3D gravity inversion and uncertainty assessment of basement relief via Particle Swarm Optimization. J. Appl. Geophys. 139, 338–350.

Poli, R., Kennedy, J., Blackwell, T., 2007. Particle swarm optimization an overview. Swarm Intell. 1, 33–57.

Shi, Y., Eberhart, R.C., 1998. Parameter selection in particle swarm optimization. Int. Conf. Evolution. Program. 591–600.

Sun, W., Okubo, S., Fu, G., Araya, A., 2010. General formulations of global co-seismic deformations caused by an arbitrary dislocation in a spherically symmetric earth model-applicable to deformed earth surface and space-fixed point. Geophys. J. R. Astron. Soc. 177, 817–833.

Swenson, S.C., Chambers, D.P., Wahr, J., 2008. Estimating geocenter variations from a combination of GRACE and ocean model output. J. Geophys. Res. 113.

Tanaka, Y., Heki, K., 2014. Long- and short-term postseismic gravity changes of megathrust earthquakes from satellite gravimetry. AGU Fall Meeting 5451–5456.

Tanaka, Y., Heki, K., Matsuo, K., Shestakov, N.V., 2015. Crustal subsidence observed by GRACE after the 2013 Okhotsk deep-focus earthquake. Geophys. Res. Lett. 42, 3204–3209. http://dx.doi.org/10.1002/2015gl063838.

Tenzer, R., Chen, W., Tsoulis, D., Bagherbandi, M., Sjoberg, L., Novak, P., Jin, S.G., 2015. Analysis of the refined CRUST1.0 crustal model and its gravity field. Surv. Geophys. 36 (1), 139–165. http://dx.doi.org/10.1007/s10712-014-9299-6.

Tsang, L.L.H., Hill, E.M., Barbot, S., Qiu, Q., Feng, L., Hermawan, I., Banerjee, P., Natawidjaja, D.H., 2016. Afterslip following the 2007 Mw8.4 Bengkulu earthquake in Sumatra loaded the 2010 Mw7.8 Mentawai tsunami earthquake rupture zone. J. Geophys. Res. Solid Earth 121.

Wahr, J., Molenaar, M., Bryan, F.O., 1998. Time variability of the Earth's gravity field: hydrological and oceanic effects and their possible detection using GRACE. J. Geophys. Res. 103, 30205–30229.

Wahr, J., Swenson, S.C., Velicogna, I., 2006. Accuracy of GRACE mass estimates. Geophys. Res. Lett. 33.

Wang, L., Shum, C.K., Simons, F.J., Tassara, A., Erkan, K., Jekeli, C., Braun, A., Kuo, C., Lee, H., Yuan, D.-N., 2012. Coseismic slip of the 2010 Mw 8.8 Great Maule, Chile, earthquake quantified by the inversion of GRACE observations. Earth Planet. Sci. Lett. 335–336, 167–179. http://dx.doi.org/10.1016/j.epsl.2012.04.044.

Wang, L., Wang, R., Roth, F., Enescu, B., Hainzl, S., Ergintav, S., 2009. Afterslip and viscoelastic relaxation following the 1999 M 7.4 İzmit earthquake from GPS measurements. Geophys. J. Int. 178, 1220–1237.

Wang, R., Parolai, S., Ge, M., Jin, M., Walter, T.R., Zschau, J., 2013. The 2011 Mw 9.0 Tohoku earthquake: comparison of GPS and strong-motion data. Bull. Seismol. Soc. Am. 103, 1336–1347.

Wang, R., Xia, Y., Grosser, H., Wetzel, H.U., Kaufmann, H., Zschau, J., 2004. The 2003 Bam (SE Iran) earthquake: precise source parameters from satellite radar interferometry. Geophys. J. Int. 159, 917–922.

Xu, C., Ding, K., Cai, J., Grafarend, E.W., 2009. Methods of determining weight scaling factors for geodetic–geophysical joint inversion. J. Geodyn. 47, 39–46.

Zhang, G., Shen, W., Xu, C., Zhu, Y., 2016. Coseismic gravity and displacement signatures induced by the 2013 Okhotsk Mw8.3 earthquake. Sensors 16, 1410. http://dx.doi.org/10.3390/s16091410.

Zhou, X., Sun, W.K., Fu, G.Y., 2011. Gravity satellite GRACE detects coseismic gravity changes caused by 2010 Chile M(w)8. 8 earthquake. Chin. J. Geophys. 54, 1745–1749.